Online Monitoring of the Final, Divergent Growth Phase in the Step-Growth Polymerization of Polyamines

Ray S. Farinato,‡ Joe Calbick,‡ Gina A. Sorci,‖ Fabio H. Florenzano,§ and Wayne F. Reed*,†

Physics Department, Tulane University, New Orleans, Louisiana, Cytec Industries, Inc., 1937 W. Main St., Stamford, Connecticut, and Universidade do Vale do Sapucaí - UNIVÁS, Pouso Alegre -MG-Brazil - 37550-000

ABSTRACT: Using automatic, continuous online monitoring of polymerization reactions (ACOMP) the final, divergent growth phase (FDGP) of the condensation polymerization of dimethylamine, epichlorohydrin, and ethylenediamine was monitored, which produced a highly ramified, polyelectrolytic polyamine. The weight average mass, M_w, increased exponentially during the FDGP, whereas weight averaged intrinsic viscosity $[\eta]_w$ increased slowly, reaching a plateau. Multi-detector gel permeation chromatography (GPC) revealed that polymers of mass 20 000 to 10^6 are branched and self-similar, but above this mass, $[\eta]$ increases less strongly with M. This appears to be due to higher order ramification, a precursor to gelation. The ACOMP trends in M_w and $[\eta]_w$ provide direct online evidence of this process. It is shown computationally that a mere increase in polydispersity cannot explain this behavior. GPC showed the mass distribution becomes highly asymmetric as conversion increases. A plausible kinetic model for the distribution asymmetry is introduced, and a complementary model for the effects of higher order ramification on $[\eta]_w$.

Introduction

Polyamines (PA) are used extensively in the water purification industry. While the step growth polymerization process to manufacture these was successfully developed in the 1960s, little effort has been devoted to understanding the kinetics and physical properties of these polyelectrolytes.

The category of polyelectrolytes referred to as polyamines encompasses a wide array of chemistries that can result from either free-radical chain growth, step growth, or derivatization reactions on preformed polymers.[1,2] The general features of this class of cationic polyelectrolytes include the possibility to synthesize high-charge-density materials from relatively inexpensive starting materials and the ability to locate the ionogenic group in the main polymer chain. The amine functionality can be designed to be unquaternized, in which case the charge on the resulting polyion would be pH dependent, or the amine can be quaternized, in which case the polyion charge would be relatively constant over a large range of pH.

The materials studied in this paper form a commercially important subset of polyamines made by step-growth synthesis from epichlorohydrin (EPI) and dimethylamine (DMA).[3] These materials account for the majority of polyamines used in the water and wastewater treatment industry, where a central objective is the deployment of inexpensive polycationics for use in the coagulation and flocculation of suspended matter. The straightforward step-growth synthesis of polyamines from epichlorohydrin and dimethylamine (EPI-DMA) results in linear polymers of low to medium molecular

weight, with a practical upper limit of $M_w \approx 10^4$ g/mol. This limitation is likely due to competition from side reactions in the step-growth synthesis.[1] Such materials make excellent coagulants and typically operate in wastewater applications via a charge neutralization mechanism. In many applications, however, a greater polymer molecular weight would result in better efficacy. There have been a number of schemes designed to enhance the molecular weight of EPI-DMA polyamines. The approach that currently dominates commercial production, because of its economic viability, is the use of small amounts of amines of functionality greater than two in the synthesis. One example in widespread commercial use is the hexafunctional compound ethylenediamine (EDA), whose incorporation into the chain necessarily creates branching of the main chain. Augmentation of polymer molecular weight using this scheme is concomitant with a change in the polymer topology.

Efforts to commercially produce EPI-DMA and EPI-DMA-EDA polyamines having consistent properties often involve a reliance on bulk solution rheology as a guide to the extent of reaction and as an index of when to quench the step-growth polymerization before an intractable, cross-linked polymer results. In fact, specifications of commercial products are often quoted in terms of solution bulk viscosities. More sophisticated analyses of molecular weight distribution and structure are mainly done offline, and do not readily allow for a rapid enough feedback for control purposes during the important final stages of the polymerization.

One has only to look at the overall features of a gel permeation chromatography (GPC) trace of an EPI-DMA-EDA polyamine to realize that a single shear viscosity value cannot capture the full suite of features that can be used to describe these materials. As seen below, while the EPI-DMA polyamines in the 10^4-10^6 mass range display monomodal GPC traces, the EPI-DMA-EDA polyamines often present multimodal, or at

* Author to whom correspondence should be addressed.
† Tulane University.
‡ Cytec Industries, Inc.
§ Universidade do Vale do Sapucaí.
‖ Current Address: Physics Department, Milsaps College, Jackson, MS.

Table 1. Experimental Conditions

reaction no.	[EDA] mol%	EPI and water additions
01	1.53	21.34 g at 4085 s
02	1.53	14.89 g at 5185 s, 6.562 g at 8458 s, 1.542 g at 19 555 s
03	1.53	21.337 g at 4709 s, 7.145 g at 7719 s
04	0.95	14.3 g at 2284 s, 7.06 g at 6807 s, 7.15 g at 10 064 s, 7.152 g at 11 865 s
05	2.13	14.257 g at 3835 s, 7.143 g at 6531 s, 1.0471 g at 17 043 s, 0.5273 g at 25 030 s, 0.6167 g at 26 760 s, 113.0 g water at 29 447 s, 3.36 g at 31 758 s
06	1.28	21.343 g at 5647 s, 1 g at 14 095 s, 1.1 g at 15 557 s, 2.116 g at 17 100 s, 50.0 g water at 17 934 s, 3.43 g at 19 078 s
07	1.85	21.304 g at 2372 s, 2.122 g at 4430 s, 2.230 g at 6209 s

least highly asymmetric GPC traces that evolve significantly throughout the later stages of the polymerization. This has several intriguing aspects. For example, one might naively expect that if the branching agent were uniformly incorporated into the growing polymer chains, then the statistical result of the polymerization would produce a broad but monomodal distribution on a GPC trace. This is obviously not the case. To unravel some of the complexities of this system, a combination of methods have been used in this work to both monitor the reaction during the step-growth polymerization, and to characterize the various stages of the reaction in a more traditional offline manner. A kinetic model and complementary higher order ramification model are introduced to rationalize the combined GPC and ACOMP trends.

This work uses two recently developed techniques for following the final divergent growth phase (FDGP) of the polyamine step-growth reaction and for characterizing the polyelectrolyte properties of the PA. Automatic continuous online monitoring of polymerization reactions (ACOMP) was introduced by Florenzano et al.[4] in 1998 and was first used to follow the chain-growth reaction of vinyl pyrrolidone. Subsequently, it has been used to monitor chain transfer kinetics,[5] continuous reactors,[6] controlled radical polymerization,[7] detailed kinetics of acrylamide reactions,[8] composition, sequence length, and mass distribution in free radical copolymerization[9] and copolymer composition profiles in nitroxide-mediated controlled radical gradient copolymerization.[10] ACOMP uses no chromatographic columns or separation techniques. Strategies for obtaining online measures of polydispersity were recently presented.[11]

Automatic continuous mixing (ACM) is an efficient and accurate means of determining equilibrium properties of polymers and multicomponent polymer/colloid solutions. It was recently introduced in the context of determining association properties of micelles and water-soluble polymers[12] and for detailed studies of properties of linear polyelectrolytes.[13-15]

The focus of this work was to elucidate the physical structure of the macromolecules that develop during the final stages of the condensation polymerization of EPI-DMA-EDA. This final stage of the reaction is the most difficult to control in a manufacturing scenario and provided the greater challenge in terms of polymer characterization. Experience dictated the protocol of adding EPI in several stages in order to avoid gelation of the sample, allowing efforts to concentrate on characterization of the final portion of the conversion sequence. That is, the condensation reaction was first carried out to ~98% conversion, during which time the polymer structure was not measured in detail. This material constituted the starting point for the final stage polymerization, which was the subject of this detailed online characterization.

It is beyond the scope of this work to review and critically compare the huge literature on branched polymers to find relevant descriptions for the results of this work. Hence, a simple conceptual model will be given at the end of this work that concisely captures the salient features of the asymmetry in the molecular weight distribution due to branching in the latter stages and also provides an intuitively appealing interpretation. Theoretical and experimental work showing precedents for such asymmetry are cited. Classic work on branching was done by Flory[16] and Stockmayer[17,18] and has seen continuous, vigorous expansion over the past 50 years, including reviews,[19] analytical calculations,[20-24] and numerical calculations, with particular attention devoted to finding methods to dramatically reduce polydispersity in branched polymer synthesis.[25-28] The relationship between branching and gelation has also been treated in depth.[29-31] Characterizing branching using GPC and light scattering and/or viscometry is still being vigorously developed.[32,33]

Materials and Methods

Polyamine Reactions. The polyamine was synthesized in water with a 3:7 ratio of solvent to monomeric material at 79 °C. This was a step copolymerization between DMA, EPI, and EDA. The EDA is used as a branching agent and is incorporated at different percentages (0.95-2.13%, by weight) into the reaction. This allows for observation of various degrees of branching. The initial reaction is taken up to 98% conversion, which produces a molecular weight of approximately 5000 g/mol. The conversion was computed on the basis of the stoichiometry of the components added. Since the EDA is added at the beginning of the reaction, it is believed that the branching occurs early on in the polymerization. If these reactions are allowed to proceed too far, there will be massive cross-linking and eventually the formation of a macroscopic gel. This is controlled by the addition of HCl, which stops the reaction. These reactions are well documented in refs 1-3.

The first 98% of conversion ('backbone' solution) was performed at Cytec Industries (Stamford, CT). The various backbone solutions with varying EDA percentages were shipped to the ACOMP lab at Tulane University where the last few percent of conversion was monitored. These solutions were placed in a reactor heated to 79 °C. A 9 g injection of NaOH was added to the 750 g of the backbone solution in the reactor to change the pH so that the reaction could proceed. This took ~30 min. To begin the ACOMP monitoring on a reaction, a baseline of the solvent and this solution were passed through a series of detectors. Once the baselines for the detectors were collected, the EPI additions began and the reaction proceeded toward completion, during which time it was continuously monitored. A variety of EPI addition sequences were used, as seen in Table 1. The amounts of EPI added were chosen on the basis of experience to avoid gelation of the reaction mixture. The addition sequence was varied in order to determine its effect on the mass evolution.

ACOMP. ACOMP has been detailed previously (refs 4–10). Briefly, it involves automatically and continuously withdrawing a sample stream from the reactor and diluting the sample stream to the level where absolute light scattering and other measurements can be made on it. The detectors included a home-built seven angle flow-through light scattering detector (this is the prototype of the Brookhaven Instruments BI-MwA), a home-built single capillary viscometer, previously described in detail,[34] and a Waters 410 differential refractometer (RI).

In this work, because of the high viscosities attained, the extraction/dilution system consisted of combined low- and high-pressure mixing stages. A total of five pumps were used to feed the low-pressure chamber from the reactor, provide for initial dilution and liquid level control, and achieve a final dilution of about 1:500 in the final high-pressure mixing stage. The diluent was a moderate ionic strength aqueous solution of 0.1 M NaCl, chosen to shield the strong polyelectrolyte effects of the PA, which are pronounced in aqueous solution at low ionic strength, as shown below.

The diluted sample, with a solute concentration typically 0.002 g/mL or less, was pumped through an online filter (0.45 μm), and the detector train. All detector signals were fed through an A/D converter and collected using home-written software. The RI was used to monitor polymer concentration, the pressure drop across the capillary yielded the reduced viscosity, and the seven angles of intensity light scattering data were used to determine the values of M_w and z-average mean square radius of gyration $\langle S^2 \rangle_z$ of the polymer as a function of time. The average lag time between a sample being withdrawn from the reactor and reaching the light scattering detector was typically 20 min and is purely a function of the ACOMP plumbing.

Gel Permeation Chromatography (GPC). The GPC system used 0.05 M Tris, pH = 7, 0.15 M Na_2SO_4, and a Shodex 806 column, an Agilent 1100 pump, Shimadzu RI, home-built single capillary viscometer and a seven-angle Brookhaven BI-MwA light scattering unit. The flow rate was 0.8 mL/min.

Dynamic Light Scattering (DLS). A Brookhaven Instruments 90 Plus was used for DLS. Data were collected at a scattering angle of 90° at an incident laser wavelength of 660 nm. The electric field autocorrelation function was computed from the intensity autocorrelation function using the standard Gaussian approximation.[35]

Evaluation of Light Scattering Data. The usual Zimm approximation for the excess Rayleigh scattering ratio $I_R(c,q)$ is the starting point for most of the light scattering analysis,[36]

$$\frac{Kc}{I_R(c,q,)} = \frac{1}{MP(q)} + 2A_2c + [3A_3Q(q) - 4A_2^2MP(q)(1 - P(q))]c^2 + O(c^3) \quad (1)$$

where c is the polymer concentration (g/cm³), $P(q)$ the particle form factor, q is the amplitude of the scattering wave-vector $q = (4\pi n/\lambda)\sin(\theta/2)$, where θ is the scattering angle, and K is an optical constant, given for vertically polarized incident light by

$$K = \frac{4\pi^2 n^2 (\partial n/\partial c)^2}{N_A \lambda^4} \quad (2)$$

where n is the solvent index of refraction, λ is the vacuum wavelength of the incident light, N_A is Avogadro's number, and $\partial n/\partial c$ is the differential refractive index for the polymer in the solvent. $Q(q)$ involves a sum of complicated Fourier transforms of the segment interactions that define A_2. In the limit of $q = 0$, $P(0) = Q(0) = 1$, so that, for a polydisperse polymer population, this becomes

$$\frac{Kc}{I_R(c,0)} = \frac{1}{M_w} + 2A_2c + 3A_3c^2 + O(c^3) \quad (3)$$

For low enough concentrations that the c^2 term in eq 1 is negligible, and for $q^2\langle S^2\rangle_z < 1$, another, frequently used form of the Zimm equation is

$$\frac{Kc}{I_R(c,q)} = \frac{1}{M_w}\left(1 + \frac{q^2\langle S^2\rangle_z}{3}\right) + 2A_2c \quad (4)$$

The value $\partial n/\partial c = 0.202$ for PA was used.[37] The methods of computing $I_R(q,c)$ from the raw data from the seven-angle light scattering unit have been amply documented (refs 4–7).

Viscosity Computation. The voltage $V(t)$ of the single capillary viscometer is directly proportional to the total viscosity of the solution flowing through the capillary. This allows the reduced viscosity η_r to be computed at each instant, without any calibration factor, according to

$$\eta_r(t) = \frac{V(t) - V(0)}{V(0)c(t)} \quad (5)$$

where $V(0)$ is the viscometer voltage when pure solvent flows. The weight average intrinsic viscosity $[\eta]_w$ is related to η_r according to

$$\eta_r = [\eta]_w + \kappa_{H1}[\eta]_w^2 c_p + O(c_p^2) \quad (6)$$

where κ_{H1} is ~0.4 for neutral polymers.[38] Shear rates in the capillary viscometer were on the order of 500 s⁻¹. It is important to note that in this work, ACOMP measurements were made at $c_p \leq 0.002$ g.cm³. Also, $[\eta]$ as determined by GPC never exceeded 60 cm³/g. Hence η_r was never more than 5% larger than $[\eta]$, and normally much smaller. So in the ACOMP experiments it will be assumed that $\eta_r \approx [\eta]_w$.

Often, there is a relationship between M and $[\eta]$ of the form

$$[\eta] = BM^b \quad (7)$$

that can be found using GPC. If $b < 0.5$, this normally indicates that branching is present since random coils usually show $0.5 \leq b \leq 0.8$. Without the fractionation afforded by GPC, the relationship between M_w and $[\eta]_w$ of the unfractionated polymer can be quite different than eq 7.

Results

Equilibrium Characterization by ACM. Before characterizing a reacting system using the ACOMP method, the solution characteristics of several DMA-EPI-EDA polymer solutions in equilibrium, quenched at various degrees of conversion, were determined offline using automatic continuous mixing (ACM). Figure 1 shows examples of data for the ACM determination of the M_w, A_2, A_3, and $[\eta]$ values of PA samples in 0.1 M NaCl, which were taken at different stages of the FDGP from experiment 06 in Table 1. The lowest conversion sample studied was ~98% converted. The rest of the samples were advanced beyond this to increasing amounts by means of reacting with an additional amount of EPI. The light scattering data are expressed as $Kc/I_R(q = 0,c)$ vs c, the PA concentration, and analyzed by quadratic fits to eq 3. The strong upward curvature shows the effect of A_3. The inset shows the simultaneous ACM viscosity determinations. Table 2 summarizes the properties of PA at the different times the aliquots were withdrawn. The dependence of A_2 on M_w was found to be
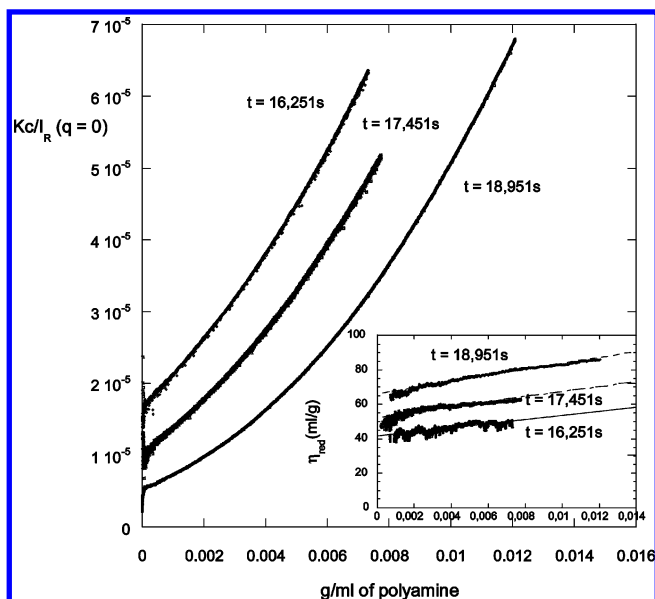
$$A_2 = 1.257M^{-0.566} \quad (8)$$

Figure 1. Results of ACM for PA aliquots withdrawn from a typical reaction 06 and quenched at different late conversion times. The solvent was 0.1 M NaCl. The main figure shows Kc/I_R ($q = 0,c$), which allows determination of M_w, A_2, and A_3. The inset shows results for η_r for the same experiments, whence $[\eta]_w$ is determined.

Table 2. Results of ACM Analyses (in 0.1 M NaCl) of DMA-EPI-EDA Polyamine at Different High Degrees of Conversion from Experiment 06[a]

time (s)	M_W (g/mol)	A_2 (mL mol/g[2])	A_3 (mL mol/g[2])	R_{eq} (Å) (eq 9)	$\langle S^2 \rangle^{1/2}$ (Å)	$[\eta]$ (mL/ g)	κ	ACOMP M_W (g/mol)
10700	4×10^4	0.0039	0.107	85	73	37	0.68	3.3×10^4
16251	5.9×10^4	0.0025	0.108	95	87	42	0.15	5.9×10^4
17451	9.6×10^4	0.0019	0.100	120	110	53	0.14	9.4×10^4
18951	17.9×10^4	0.0011	0.103	152	145	65	0.27	17.6×10^4

[a] The last column shows corresponding ACOMP measure of M_w.

This is an unusually strong mass dependence for A_2 but is expected for branched/cross-linked polymers since

$$A_2 = \frac{N_A}{M^2} \frac{16\pi R_{eq}^3}{3} \tag{9}$$

where R_{eq} is proportional to $\langle S^2 \rangle^{1/2}$ and R_{eq} is the equivalent excluded volume radius of the polymer. R_{eq} computed from eq 9 (with $M = M_w$) is given in Table 2. Furthermore

$$\langle S^2 \rangle^{1/2} = AM^a \tag{10}$$

where a is typically 0.4−0.5 for branched/cross-linked polymers, yielding an expected A_2 mass exponent of −0.5 to −0.8. Such values have been often found.[39]

The strong polyelectrolyte nature of PA was observed by ACM, where A_2 varied from 0.03 to 5×10^{-4} (cm³ mol)/g² over the ionic strength range of 1−100 mM (data not shown).

An important cross-check that was made must be mentioned here: A priori, shear thinning of the polymer during ACOMP could lead to downward curvature of η_r vs M_w. This possibility was excluded, however, by measuring η_r vs shear rate over 2 orders of magnitude, up to 7000 s⁻¹, for final PA solutions at the ACOMP detection concentration of 0.0022 g/cm³. There was no variation in η_r over this range of shear rate. Furthermore, at a given shear rate, there was little difference
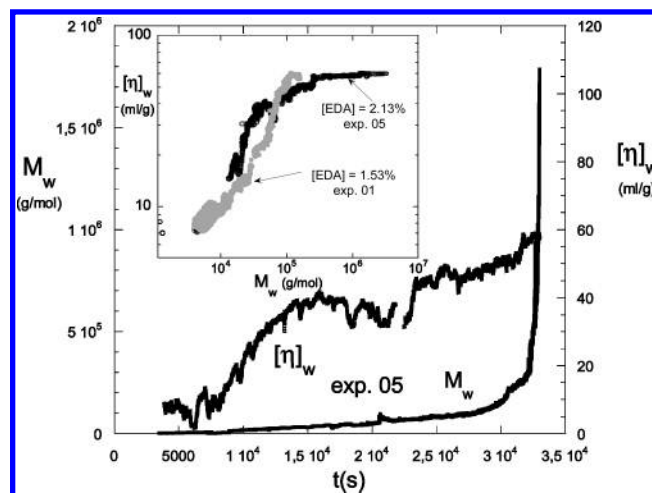

Figure 2. ACOMP results for $[\eta]_w$ and M_w for experiment 05 in Table 1. The divergence of M_w is striking, whereas $[\eta]_w$ follows a slow increase with an inflection point and subsequent negative second time derivative. The inset shows $[\eta]_w$ vs M_w for the same data.

in η_r over 2 orders of magnitude in concentration, from 2×10^{-3} g/cm³ (in ACM and ACOMP) to about 2×10^{-5} g/cm³ (i.e., in GPC). Given the extremely low values of $[\eta]_w$ for PA endproducts, typically around 30 cm³/g, the lack of shear thinning is not surprising, as it is more usually found in polymers of both high M_w and high $[\eta]_w$, such as high M_w polyacrylamide.[40,41] On the basis of the shear and concentration independence of η_r, in the rest of this work, η_r is taken to be identical with the weight average intrinsic viscosity $[\eta]_w$.

In light of the ACM polyelectrolyte results, it was decided that a 0.1 M NaCl solution provided good shielding of polyelectrolyte charges for subsequent ACOMP experiments and that concentrations of up to 0.002 g/mL in the diluted ACOMP stream would be acceptable.

ACOMP of the Final Divergent Growth Phase (FDGP). Table 1 summarizes reaction conditions for seven different experiments. Figure 2 shows M_w and $[\eta]_w$ vs t for reaction 05 in Table 1. The data represent approximately the last 2% of the conversion of polyamine. The M_w values were corrected for A_2 at each point in eq 3, using the following iterative scheme: First, the uncorrected M_w (i.e., the M_w found by first taking $M_w \approx I_R(q = 0,c)/Kc$) was used in the A_2 equation to find an A_2 value, whence a new value of M_w was computed and a subsequent value of A_2 recomputed. This was continued until M_w no longer changed noticeably, usually about 10 iterations. The two most striking features of the Figure 2 data are (1) the divergence of M_w toward the very end of the reaction and (2) the downward concavity of $[\eta]_w$ over the same latter period. These data provide strong evidence of changing population characteristics during this final portion of the reaction, which dramatically change the scaling behavior between M and $[\eta]$. From a practical point of view, they reveal that reduced viscosity measurements alone are not a good means to monitor M_w since the branching prevents viscosity from rising sharply and following M_w. The inset to Figure 2 shows $\log[\eta]_w$ vs $\log(M_w)$. There is no single scaling law apparent, and the instantaneous slope decreases and becomes essentially zero at high values of M_w.

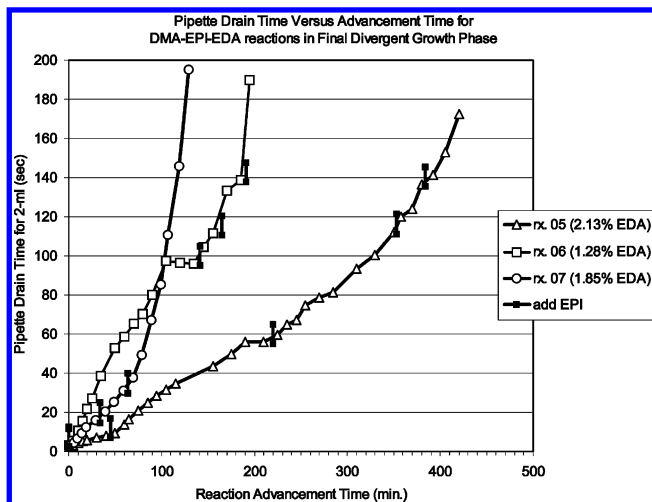The ACOMP data for M_w and $[\eta]_w$ vs time for the other reactions from Table 1 showed similar trends

Figure 3. Pipet drain times (seconds for 2 mL) as a function of reaction time during the final advancement stage (>98%) of DMA-EPI-EDA polyamines made with 1.28 (reaction 06), 1.85 (reaction 07), and 2.13 (reaction 05) mol% EDA.

Figure 4. $\langle S^2 \rangle_z$ vs M_w for reaction 03. The inset shows the slope, $d(Kc/I_R)/d(q^2)$ vs time during the FDGP. The increase of this slope corresponds to increasing polydispersity.

(data not shown). The most salient feature was that for all values of [EDA] $\geq$ 1.28%, M_w rises exponentially in the latter portion of the reaction. For [EDA] = 0.95, reaction 04, the reaction proceeded to a final value of 20 000 g/mol and stopped. Hence, it appears there is a threshold value of [EDA] below which there is not the critical number of branch points necessary for higher-order ramification.

ACM data for aliquots withdrawn at different points during reaction 06 are summarized in Table 2. The agreement between M_w obtained by ACOMP and ACM is excellent and shows that what is measured in the ACOMP detectors after the automatic extraction and dilution process is the same as what is measured from reaction aliquots withdrawn from the reactor, immediately cooled and diluted (and, hence, quenched), and then measured.

Figure 3 shows relative bulk viscosity (expressed as pipet drain time) vs t for three reactions. The pipet drain time is a rough-and-ready measure of the advancement of the polyamine reaction, and the processability of the polymer solution (i.e., whether it can still be pumped out of the reactor). The evolution of the pipet drain time with advancement time will not only depend on the composition of the prepolymer (backbone polymer) but also on the sequence and timing of additional amounts of EPI added to further the reaction. This can be clearly seen in Figure 3. The various additions of EPI are noted in the figure, and the exact amounts added are quoted in Table 1.

Figure 4 shows $\langle S^2 \rangle_z$ vs M_w for reaction 03, computed from eq 4 (note that this is mean squared radius, not the root-mean-square). The change in slope resembles the behavior of the log(η_r) vs log(M_w) inset in Figure 2, in that it decreases steadily with M_w. The inset shows the slope of eq 4, $d(Kc/I_R)/d(q^2)$, vs t. This is equal to

$$\frac{d(KC/I(q))}{d(q^2)} = \frac{\langle S^2 \rangle_z}{3M_w} \quad (11)$$

Using eq 10, where $a = a(M)$ and runs from 1/3 for dense spherical, objects, to 0.5 for ideal coils, to 0.6 for random coils with excluded volume, reveals that the slope is a
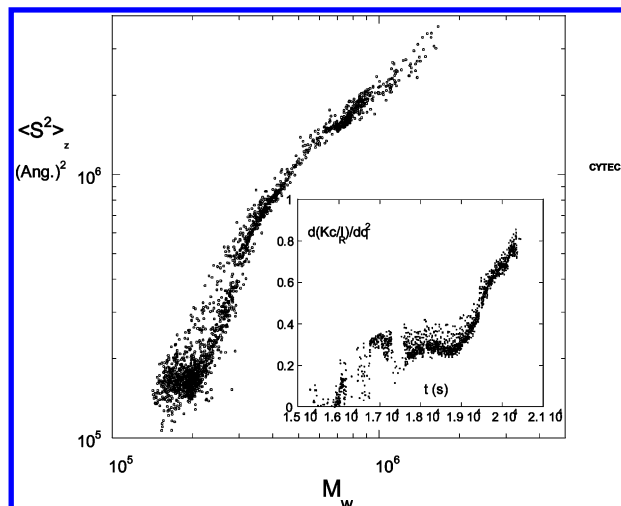
direct measure of the following moments of the polymer mass distribution

$$3 \times \text{Slope} = \frac{B \int M^{2a(M)+1}c(M)\,dM/\int Mc(M)\,dM}{\int Mc(M)\,dM/\int c(M)\,dM} \quad (12)$$

The numerator is hence a rather peculiar average of M but becomes M_z for ideal coils, making the slope proportional to M_z/M_w. The numerator measures something somewhat less than M_z for branched molecules. Since $a(M)$ may be decreasing, as seen in Figure 4 and its inset, the average that $3 \times$ Slope measures will be progressively less than M_z/M_w. The fact that the slope increases is hence a strong indication of increasing polydispersity.

The major question at this point is why M_w diverges, while $[\eta]_w$ levels off in the FDGP. Several possibilities present themselves. Perhaps the polymers become more branched/cross-linked in the FDGP, changing the scaling relationships of eqs 7 and 10, while the population continues to be essentially unimodal, as predicted by basic step-growth theory. Perhaps the increasing polydispersity revealed by the slope in eq 11 is alone sufficient to cause a significant change in the M_w and $[\eta]_w$ relationship, even without changing the relationship of eq 7. It is also possible that other population 'modes', with different M_w and $[\eta]_w$ relationships are produced in the FDGP, breaking the strict unimodality of ideal step growth.

ACOMP alone is unable to distinguish between these possibilities. Hence, GPC measurements are presented below.

GPC Results. Figure 5 shows raw light scattering (90°) and RI chromatograms of PA aliquots withdrawn at different times during reaction 06 with 1.28% EDA. The initial aliquot (1a) gives a fairly symmetric unimodal RI signature, with low light scattering. Successive aliquots show a second 'mode' growing in, seen as a large RI shoulder at low elution volumes, and a well-defined light scattering peak that moves toward lower elution volumes as the reaction proceeds. It is tempting to identify the second mode with a growing population of polymer having a different chain architecture than the polymer in the principal RI peak.
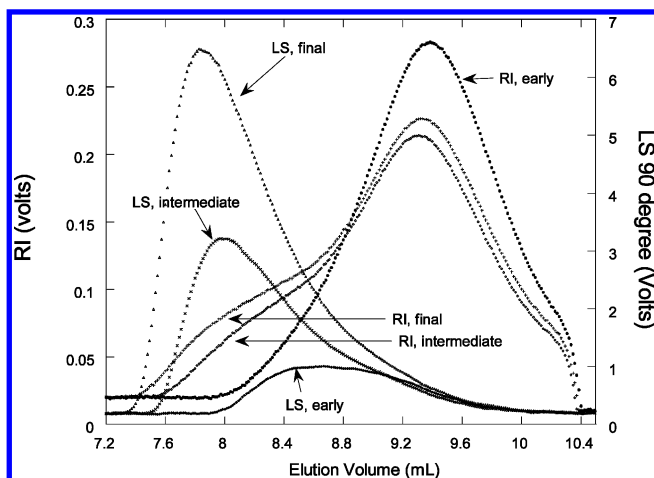
Figure 5. Raw RI and 90° LS chromatograms for aliquots of PA withdrawn at different stages of the FDGP for 06.

Table 3. GPC Characteristics of Aliquots Withdrawn during Reaction 06

aliquot withdrawal time (s)	M_w	M_{peak}	M_η	M_w/M_n	M_z/M_w
600	6.6×10^4	3.1×10^4	4.4×10^4	3.5	3.2
1500	7.3×10^4	3.1×10^4	5.0×10^4	4.1	3.5
4200	14.5×10^4	4.0×10^4	8.7×10^4	6.6	4.7
8400	23.1×10^4	4.4×10^4	12.6×10^4	9.7	5.5
9900	25.5×10^4	4.2×10^4	14.5×10^4	9.9	5.5
17 100	34.8×10^4	4.8×10^4	16.5×10^4	12.5	6.0
18 900	41.4×10^4	5.3×10^4	15.9×10^4	12.8	5.9

Table 3 shows the various GPC analysis parameters for reaction aliquots of experiment 06; M_w, M_w/M_n, etc. The polydispersity indices M_w/M_n and M_z/M_w increase significantly during the polymerization due chiefly to the build-in of the second mode. Whereas M_w increases over 7-fold for the aliquots studied, the peak value of the mass distribution M_{peak}, rooted firmly in the original low mass mode, increases by less than a factor of 2.

One normally expects a geometrical distribution to describe an ideal step growth reaction

$$W(k) = (1 - p)p^{k-1} \qquad (13)$$

where $W(k)$ is the probability of a chain being k units long at conversion $p \in [0,1]$. The mass distributions, in contrast, are fairly well fit by bimodal, log-normal distributions of the form

$$\varsigma(\ln M) = \varsigma_1 \exp\left[-\omega_1\left(\ln\left(\frac{M}{M_1}\right)\right)^2\right] + \varsigma_2 \exp\left[-\omega_2\left(\ln\left(\frac{M}{M_2}\right)\right)^2\right] \qquad (14)$$

where ς (ln M) dln M is the concentration in the interval from ln M to ln M + dln M. ς_1 and ς_2 are the amplitudes of each mode, ω_1 and ω_2 the reciprocal square root of each distribution's width, and M_1 and M_2 are the peak of each distribution. $\zeta(\ln M)$ obeys the normalization condition

$$\int \varsigma(\ln M)d\ln M = C_0 = C_1 + C_2 \qquad (15)$$

where C_0 is the total concentration of polymer and C_1 and C_2 are the total concentrations of modes 1 and 2, respectively. This leads to

$$C_1 = \varsigma_1\sqrt{\pi/\omega_1}, \; C_2 = \varsigma_2\sqrt{\pi/\omega_2} \qquad (16)$$

Figure 6 shows such a fit (dashed line) for the final aliquot of reaction 02. In fact, this approximation is robust for *all* GPC measurements made, on all of the reactions, both for end products, and aliquots removed and quenched during the FDGP. It is not obvious that the second Gaussian fit by eq 14 is actually a separate 'mode' of qualitatively different PA. The bimodal log-normal fits are, at the least, a means of representing the population and exploring the consequences in a concise mathematical form. Table 4 summarizes the bimodal log-normal fit parameters for the aliquots of experiment 06, the same aliquots used in Table 3.

Figure 6 also shows [η] vs M for the data. This behavior is typical of all the final products. It is remarkable that for a given end product [η] vs M follows the same scaling law for 2 orders of magnitude in mass for which the exponents b in eq 7 vary from 0.35 to 0.48, all of which are characteristic of branched polymers. This means that all the polymers throughout the distribution are branched, at all masses down to at least around 20 000, and that the branched polymeric architecture is self-similar up to about 10^6. For $M > 10^6$, there is clear downward curvature for the log [η] vs log M data. As seen, there is a meaningful amount of eluting polymer in this regime to render the [η] data reliable. The trend shows that the self-similarity breaks down and that material in this regime follows a different [η] vs M relationship.

It is also notable that [η] for the high M_w PA are much lower than for typical unbranched, neutral polymers, e.g., polyacrylamide of $M \approx 10^6$ has [η] $\approx$ 300 cm³/g,[22,23] and poly(vinyl pyrrolidone) for $M \approx 10^6$ has [η] $\approx$ 200 cm³/g.

Another argument for the branched nature of the PA over the $M \approx 10^4-10^6$ regime can be made by assuming the PA chains are linear, computing the apparent persistence length, and demonstrating that the value so obtained is inconsistent with a linear polymer. Since $\langle S^2 \rangle$ is too small for LS measurements over the majority of the stated range, [η] can be used in conjunction with the Flory−Fox model to obtain a viscosity-based mean
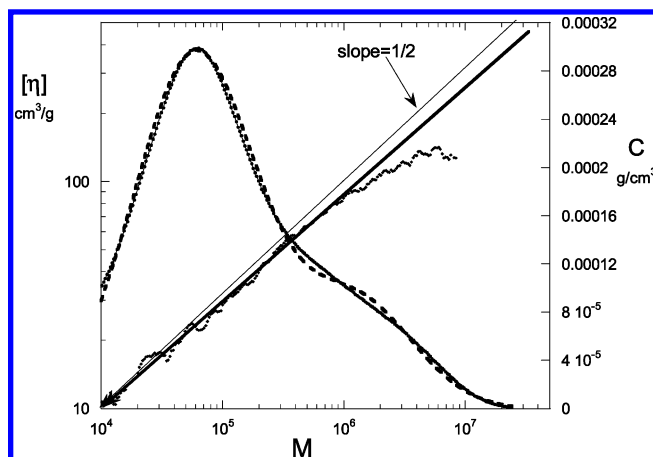

Figure 6. Fitting of a final PA mass distribution (reaction 02) with the approximation of a bimodal log-normal fit (eq 14). Also shown is log [η] vs log M for the same data, showing the decrease in the exponent b in the power law of eq 7.

Table 4. Bimodal Log-Normal Distribution Analysis for the Aliquots in Table 3, Experiment 06, with Aliquots Withdrawn at the Times Indicated[a]

aliquot withdrawal time (s)	ς_1	M_1	ω_1	M_w/M_n by $e^{1/2\omega_1}$	ς_2	M_2	ω_2	M_w/M_n by $e^{1/2\omega_2}$
600	4.35e-4	31 700	0.366	3.92	2.2e-5	4e5	3.74	1.14
2400	4.56e-4	33 800	0.360	4.0	5.06e-5	4e5	1.5	1.40
8400	3.24e-4	44 800	0.295	5.4	8.2e-5	8.6e5	0.707	2.02
17 100	3.25e-4	52 000	0.286	5.7	9.5e-5	1.21e6	0.566	2.4
18 900	3.4e-5	56 100	0.287	5.7	1.06e-4	1.33e6	0.53	2.56

[a] Polydispersity indices of each mode are computed from their respective width and by using eq 20.

square radius of gyration, $\langle S^2 \rangle_\eta$. For a coil polymer at the Θ-point[42]

$$[\eta] = \frac{\Phi_v}{M}(\sqrt{6}\langle S^2 \rangle_\eta^{1/2})^3 \qquad (17)$$

where $\Phi_v = 2.56 \times 10^{23}$. Using this idealization together with the resulting $\langle S^2 \rangle_\eta$ in the coil limit of the wormlike chain formula

$$\langle S^2 \rangle_\eta = \frac{LL_T}{3} \qquad (18)$$

yields a persistence length of 4.4 ± 0.6 Å when averaging over the stated mass range and over the endproducts of all the experiments. The apparent persistence length[43] includes excluded volume effects,[44-46] so that the true intrinsic persistence length is even smaller. Here, a contour length of the PA repeat unit of 5Å and a molar mass of 102 g/mol were used in computing the linear chain contour length L. This apparent persistence length is much lower than those for even very flexible linear polymers,[47,48] which is yet another indication that the polymers are branched/cross-linked, and not linear. If the branched chain were treated as pseudolinear in eq 18, then there would be a higher mass per unit contour length, L would be smaller, and L_T would be larger, as expected. If the same procedure is applied to masses $>10^6$, the apparent persistence length is even smaller and decreases steadily with increasing M.

For comparison with the excluded volume-based R_{eq}, $\langle S^2 \rangle_\eta^{1/2}$ is computed via eq 17 (with $[\eta] = [\eta]_w$ and $M = M_w$) and entered in Table 2. Although related, R_{eq} and $\langle S^2 \rangle_\eta^{1/2}$ are not theoretically exactly equal for coil or branched polymers. They are nonetheless very close in value in this case, as seen in Table 2.

Another important GPC observation is that M_w and $[\eta]_w$, found by integrating the GPC distributions, behave very similarly to the ACOMP trends. Notably, the inflection point of $[\eta]_w$ is seen, just as in ACOMP, as well as the steep increase in M_w.

Discussion

Here, the ACOMP data are interpreted in light of the GPC results. Again, the major ACOMP features are (1) M_w has a positive second time derivative throughout the latter stages of the reaction and diverges toward infinity near the end of the reaction, whereas (2) $[\eta]_w(t)$ normally has an inflection point during the reaction, and subsequently a negative second derivative and does not diverge, and (3) $\log M_w$ vs $\log [\eta]_w$ has a decreasing slope and so does not give a unique power law. There is a question as to whether the latter behavior is evidence for changing polymer architecture or merely due to increasing polydispersity.
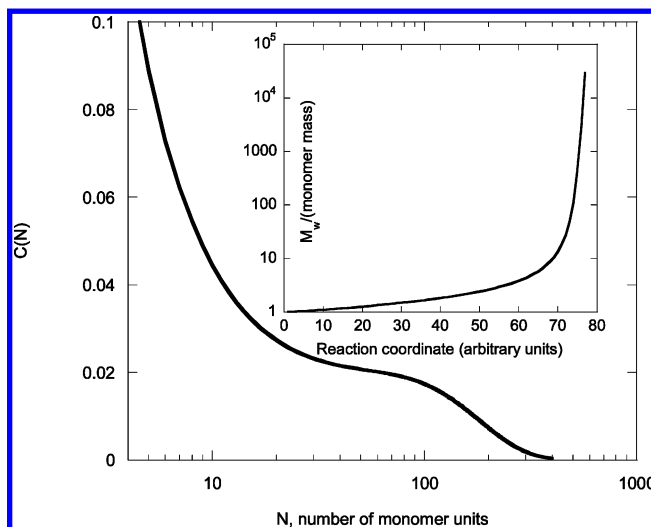

Figure 7. Model calculation of the mass distribution $C(N)$ according to the mass-weighted propagation model described in the text ($\langle n \rangle = g_1 N$). The inset shows the evolution of M_w with reaction completion, according to the mass-weighted model.

Log $[\eta]_w$ vs log M_w ACOMP behavior cannot be merely due to increasing polydispersity if the scaling relationship between $[\eta]$ and M remains unchanged. First of all, the growing asymmetry of the mass distribution during the reaction and large increase in polydispersity indices M_w/M_n, M_z/M_w (Table 3) immediately show that simple step growth is not occurring since for the governing geometric distribution (eq 13)

$$M_w/M_n = 1 + p \qquad (19)$$

and we are only interested in conversions for $p > 0.90$, so there should be no significant change in polydispersity for ideal step growth.

The log-normal distribution of eq 14 allows the effects of increasing polydispersity to be investigated computationally. The βth moment of the log-normal distribution of peak mass M_0 is easily computed

$$\langle M^\beta \rangle = \int M^\beta \varsigma (\ln M) d\ln M = M_0^\beta \sqrt{\frac{\pi}{\omega}} \exp\left[\frac{\beta^2}{4\omega}\right] \qquad (20)$$

which allows determination of M_w and $[\eta]_w$ for the bimodal distribution above:

$$M_w = \frac{\varsigma_1 M_1 \sqrt{1/\omega_1} \exp(1/4\omega_1) + \varsigma_2 M_2 \sqrt{1/\omega_2} \exp(1/4\omega_2)}{\varsigma_1 \sqrt{1/\omega_1} + \varsigma_2 \sqrt{1/\omega_2}} \qquad (21)$$

where ς_1 is the amplitude, M_1 the peak mass, and ω_1 the reciprocal square root of the width of the first log-

normal distribution, and likewise ς_2, M_2, and ω_2 for the second distribution, typical values of which during the FDGP are given in Table 4. (It is noted that computation of the polydispersity indices backward from the bimodal fit parameters yields values in reasonable agreement with those given in Table 3, found directly by fit-independent GPC analysis.)

Likewise, $[\eta]_w$ can be found in conjunction with the mass/viscosity scaling laws of the form $[\eta_1] = B_1 M_1{}^{b_1}$ and $[\eta_2] = B_2 M_2{}^{b_2}$ to be

$$[\eta]_w = \frac{\left(B_1\varsigma_1 M_1{}^{b_1}\sqrt{1/\omega_1}\,\exp[b_1{}^2/4\omega_1] + B_2\varsigma_2 M_2{}^{b_2}\sqrt{1/\omega_2}\,\exp[b_2{}^2]/4\omega_2\right)}{\varsigma_1\sqrt{1/\omega_1} + \varsigma_2\sqrt{1/\omega_2}} \quad (22)$$

In the PA reactions, C_2 grows at the expense of C_1, and the two are related to the total concentration, C_0, in the reactor (or in the solution injected into the GPC system) by eq 15. Equations 21 and 22 were used to investigate possible behaviors of M_w and $[\eta]_w$ under different bimodal scenarios and limiting conditions, whence the following conclusion comes.

The type of downward curvature of log $[\eta]_w$ vs log M_w, seen in the inset of Figure 2, cannot be the result of shifting polymeric mass from the low-mass mode to the high-mass mode in eqs 21 and 22 if the scaling relationship between $[\eta]_w$ and M_w is the same for each mode, no matter how the average mass of each mode increases in time, and no matter how the width of each distribution broadens (with the constraint, provided by GPC, that $M_{1w} < M_{2w}$). To observe the trends in $[\eta]_w$ and M_w measured during the FDGP by ACOMP, there must be a change in scaling law such that log $[\eta]$ increases less steeply with log M than in the initial $M = 10^4 - 10^6$ regime. This can only happen if $[\eta]$ begins to decrease with M at a certain point, which means the self-similarity breaks down. The model below provides a plausible scheme for this.

Conceptual Model for 'Ramifying Growth'. These considerations lead to the following conceptual model, whose kinetic and structural consequences are sketched below: Due to the incorporation of EDA from the beginning of the reaction there is, from the start, a mixture of linear and branched chains, these latter being sparse when M_w is very low, since small quantities of EDA are used (Table 2). A linear chain has two reactive centers, one at each end, to which it can add monomers and other chains. A branched polymer has more than two active centers to which to add monomers and other chains. During the slow growth period of M_w, both linear and branched chains primarily add monomers and short, linear chains, such that the number of reactive sites on a polymer after a typical addition does not increase. As M_w increases, the percentage of branched polymers increases since a fixed number of EDA sites are shared among a diminishing number of chains. Hence, in a typical addition reaction, the probability of adding a branched polymer increases as M_w increases. When this happens, the number of reactive sites on the initial polymer increases, giving it a higher chance for propagation compared to a polymer with fewer reactive sites.

Scheme 1 illustrates the conceptual model with some particular cases, where the circled stars show the addition sites, which disappear upon addition. In Scheme 1a, there is addition of monomer or a linear chain to a

Scheme 1. Particular Examples of (A) 'Linear Growth', (B) 'Steady Branch Growth', and (C) 'Ramifying Growth', According to the above Definitions.[a]
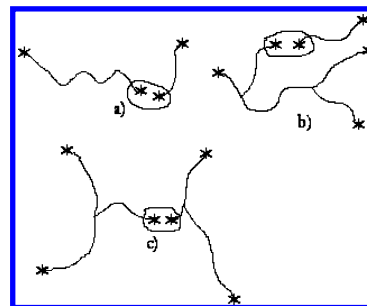
[a] (A) and (B) conserve the number of reactive sites on the larger chain after the growth step, whereas in (C) the number of reactive sites increases.

linear chain. This does not increase the number of reactive sites, which remains at two. This is termed, simply, 'linear growth'. In Scheme 1b, a branched polymer adds a monomer or a linear chain and hence grows in a way that preserves its architecture and leads to no change in the number of reactive sites, four in this case. This can be termed 'steady branch growth'. In Scheme 1c, a branched chain adds to a branched chain, leading to an net increase in the number of reactive sites, from three to four in this particular case. For the purposes of this work, this is termed 'ramifying growth',[49] to indicate the addition of branches and, hence, reactive sites. The onset of significant ramifying growth can be regarded as the onset of microgelation, which is the precursor to macroscopic cross-linking and gelation in the reactor. These notions form the basis of rudimentary kinetic and structural models.

Kinetic Model for an Evolving Multimodal Polymer Population. It is beyond the scope of this work to make refined models for the phenomena presented or to sift from the vast branching literature the best models to date to describe them. Nonetheless, the essential features of the observations can be captured with fairly simple models. These must predict the evolution of the type of bimodal (or highly asymmetric unimodal) population shown in the GPC results of Figures 5 and 6, the type of log $[\eta]_w$ vs M_w behavior seen in ACOMP (Figure 3), the $[\eta]$ vs M results in GPC (Figure 6), and the divergent behavior of M_w at high conversion (Figure 3).

Consider a polymer population in which multifunctional branch points are distributed sparsely (e.g., on the order of 1% of the initial monomer population, as per Table 2). Linear polymers have no branch points and hence two reactive ends, no matter how large their mass, M. *Branched* polymers have one or more multifunctional sites from which branches grow (i.e., two ends plus four propagating arms in the case of a hexafunctional EDA incorporated into a chain). In linear and steady branch growth, as defined above, the number of reactive sites on a polymer does not increase. Ramifying growth increases the number of reactive sites on the polymer. The first approximation is to assume the average number of propagating sites, $\langle n \rangle$, on a polymer can be represented by a power series in N, the number of monomer units in a polymer.

$$\langle n \rangle = \sum_{i=0} g_i N^i \quad (23)$$

where each coefficient $g_i \ll 1$, for $i \geq 1$. For nonramifying

growth $\langle n \rangle$ = constant (e.g., $\langle n \rangle = 2$), independent of N. The simplest approximation from eq 23 for ramifying growth is $g_i \approx 0$ for all $i \neq 1$:

$$\langle n \rangle = g_1 N \qquad (24)$$

Let $P(N)$ be the probability that a polymer in the population consists of N monomers. This is proportional to the number density of polymers with N monomers. The change in this probability when a reaction occurs is

$$\frac{dP(N)}{dr} = -\kappa \langle n \rangle P(N) \sum \langle m \rangle \, P(M) +$$
$$\kappa \sum_{L+J=N} \sum \langle l \rangle \, \langle j \rangle P(L) P(J) \quad (25)$$

where r is the reaction coordinate and κ the rate constant, assumed equal for all chain lengths and types of addition.

Using the assumption about $\langle n \rangle$ above and the fact that $C(M) = MP(M)$

$$C_0 = \sum MP(M) \qquad (26)$$

allows the above equation for $P(N)$ to be written as

$$\frac{dP(N)}{dr} = \kappa g_1{}^2 \left[\sum_{L+J=N} \sum C(L) C(J) - NP(N) C_0 \right] \quad (27)$$

i.e., the change in $P(N)$ becomes *mass* weighted as a result of ramifying growth. For linear or branched growth, as defined above, $\langle n \rangle$ does not change with N, so that the change in $P(N)$ remains *number* weighted, rather than mass weighted, and the high-mass second mode does not appear. Including terms for $i > 1$ in eq 23 could lead to changes in $P(N)$ controlled by combinations of higher moments.

The weight-averaged degree of polymerization, N_w, can be computed directly as

$$N_w = \frac{\sum N^2 P(N)}{C_0} \qquad (28)$$

Computing $dP(N)$ using increments dr allows $P(N,r)$ to be computed, where r is the number of reactions steps. The change in $P(N)$ is weighted toward higher masses because of the fact that $\langle n \rangle$ is proportional to N, and this leads to a second mode in the population, as can be seen in sample distributions computed numerically.

No attempt is made here to match actual experimental distributions or to refine eq 24. Nonetheless, the conceptual value of the model is shown in Figure 7, computed for $g = 0.02$, at high conversion. The asymmetric, high-mass mode is clear. The inset shows the divergence of M_w at high conversion, which is also found experimentally.

There is ample precedent in the literature for this type of asymmetry. Analytical functions based on the random, branched combination of Schulz–Zimm distributed primary chains have been derived which lead to similar asymmetry.[50] This approach was also generalized to arbitrary primary chain distributions.[51] A 'numerical fractionation' approach with simulation results likewise yields such asymmetry,[52] as well as the Galerkin h–p finite element method.[53] Asymmetric
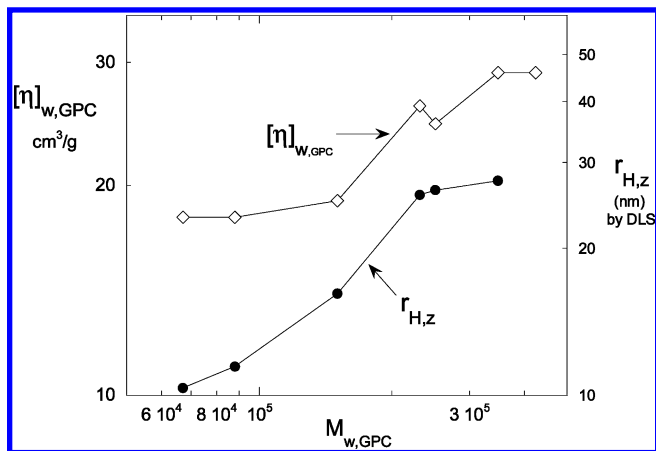

Figure 8. GPC data for $M_{w,GPC}$ and $[\eta]_{w,GPC}$ for aliquots withdrawn from the reactor at different times and quenched. Also shown are the DLS values for effective hydrodynamic radius, $r_{H,z}$, as defined in the text.

distributions were found experimentally for linking reactions using light scattering coupled to temperature gradient interaction chromatography,[54] and for branching reactions using GPC with light scattering.[55,56]

Substantiation of Trends by DLS Data. The electric field autocorrelation function $g_1(\tau)$ can be analyzed according to the standard cumulant approach,[57] where

$$\ln(g_1\tau) = c + q^2 \langle D \rangle \, \tau + \frac{\mu_2}{2} q^4 \tau^2 + \dots \qquad (29)$$

where $\langle D \rangle$ is an average of the translational diffusion coefficient of the particle, and the average shown in eq 29 is a z average, when A_2 effects are negligible and $P(q) \approx 1$. Using the Stokes–Einstein equation, this average can be represented as

$$\langle D \rangle_z = \frac{k_B T}{6\pi\eta} \left\langle \frac{1}{R_H} \right\rangle_z \qquad (30)$$

D is itself related to M at a given value of M by

$$D = HM^h \qquad (31)$$

where $h = 0.5$ for ideal coils and $h < 0.5$ for branched polymers. Using the log-normal distribution of eq 14, together with the result for $\langle M^\beta \rangle$ in eq 20, and defining $r_{H,z}$ as an effective hydrodynamic radius as follows leads to

$$r_{H,z} \equiv 1/\left\langle \frac{1}{R_H} \right\rangle_z = M_0{}^h \exp[(2h - h^2)/4\omega] \qquad (32)$$

which, for a bimodal log-normal population leads to

$$r_{H,z} = \frac{\begin{array}{l} (H_1 \varsigma_1 M_1{}^h \sqrt{1/\omega_1} \exp[(2h_1 - h_1{}^2)/4\omega_1] + \\ H_2 \varsigma_2 M_2{}^h \sqrt{1/\omega_2} \exp[(2h_2 - h_2{}^2)]/4\omega_2) \end{array}}{\varsigma_1 \sqrt{1/\omega_1} + \varsigma_2 \sqrt{1/\omega_2}} \qquad (33)$$

whose close relationship to eq 21 is evident.

Figure 8 shows $\log(r_{H,z})$ vs $\log(M_{w,GPC})$. The downward concavity of the plot is similar to that of $\log [\eta]_{w,GPC}$ vs $\log M_{w,GPC}$ shown on the same figure, which is also similar to the ACOMP plots of $\log [\eta]_w$ vs $\log M_w$. Since h should be similar in magnitude to b (eq 7), this trend

indicates that h is decreasing with M, just as b decreases, hence constituting further evidence of the change in polymer scaling relationships toward more branched forms.

Ramifying Growth Model. Several approaches to the cross-linking problem can be taken. Here, an intuitively appealing step addition of chains is sketched. It involves only one physically interpretable parameter and makes no assumptions about the relative reactivities of activated amine groups vs activated EDA groups. It also does not have to separately consider propagation by end addition vs side-chain addition. The model itself does not require any specific polymeric architecture to be valid, but in the application here, it considers the special case of a collection of random coils that have reactive end and side groups and can hence link to each other at both end and side locations.

Consider a particle of N_1 identical subunits of dimension $\langle S^2 \rangle_1$. It is easy to show that if the mean square radius of gyration is computed with respect to a point a distance X away from the centers of mass (CM), then the new value $\langle S^2 \rangle'$ is given by

$$\langle S^2 \rangle' = \langle S^2 \rangle_1 + X^2 \tag{35}$$

Now, consider a second particle consisting of N_2 of the same type of subunits as the first particle and of dimension $\langle S^2 \rangle_2$. Assume that the particles then link to each other such that their CM are at a distance X from each other. It is an elementary property of the CM that the distance of each particle from the new CM is given by

$$N_1 X_1 = N_2 X_2 \tag{36}$$

where $X = X_1 + X_2$. These facts can be used to show that the radius of gyration of this compound particle $\langle S^2 \rangle_{1,2}$ with respect to the new CM is then given by

$$\langle S^2 \rangle_{1,2} = \frac{N_1 \langle S^2 \rangle_1 + N_2 \langle S^2 \rangle_2 + \left(\dfrac{N_1 N_2}{N_1 + N_2}\right) X^2}{N_1 + N_2} \tag{37}$$

It is now possible to keep linking more particles to the preceding one using the previous value of $\langle S^2 \rangle$ of the compound particle as $\langle S^2 \rangle_1$, N_2, and $\langle S^2 \rangle_2$ for the next particle added. So far, there is no reference to any specific architecture of the particles, which can have arbitrary shapes and mass distributions. Note that in the limiting case where $X = 0$, $N_1 = N_2$, and $\langle S^2 \rangle_1 = \langle S^2 \rangle_2$ there is no change in $\langle S^2 \rangle$. This corresponds to packing polymer chains into a fixed spatial volume, which is one kind of microgelation.

To apply this general expression to any given problem requires only that a model of $P[X(n)]$ be made, where $P[X(n)]$ represents the normalized probability of a given value of X occurring after n particles have been joined together. Then, for the nth particle added, the average value of $\langle S^2 \rangle_{1,2}$, represented by $\langle\langle S^2 \rangle\rangle(n)$ is given by

$$\langle\langle S^2 \rangle\rangle(n) = \int \langle\langle S^2 \rangle_{n-1,2} \rangle P[d(n)] dX \tag{38}$$

In the ACOMP experiments, average values are measured, so that $P[X(n)]$ is not directly measurable but $\langle\langle S^2 \rangle\rangle(n)$ and quantities related to $\langle S^2 \rangle$, such as hydrodynamic volume, are directly measured. Hence, in the following, X will represent the average value of X that
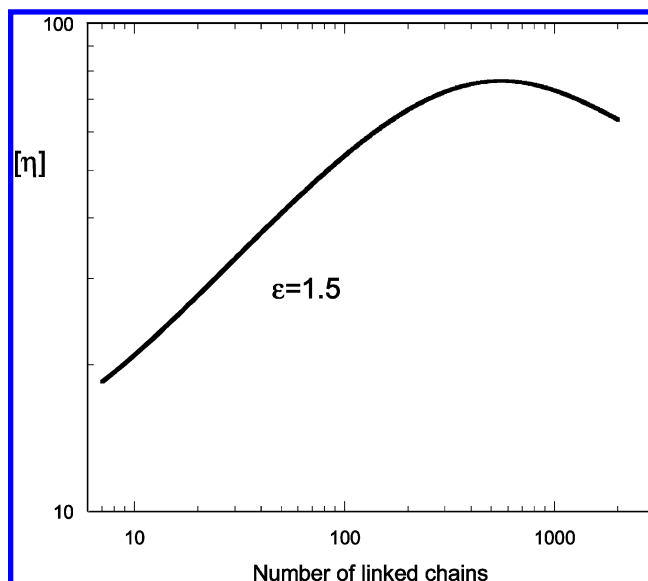

Figure 9. Sample computation of $[\eta]$ vs N (no. of chains linked) according to the cross-linking model described in the text, with $\epsilon = 1.5$.

would result when applying the theorem of the mean to the above integral.

In adapting the model to ideal random coils, a dimensional argument for modeling X is to assume that X^2 will be some multiple, ϵ, of the sum of the individual $\langle S^2 \rangle$;

$$X^2 = \epsilon(\langle S^2 \rangle_1 + \langle S^2 \rangle_2) \tag{39}$$

we can solve eq 39 to find that $\epsilon = 2$ in the limiting case of end-to-end addition of ideal linear coils, for which $\langle S^2 \rangle_{1,2} = \langle S^2 \rangle_1 + \langle S^2 \rangle_2$. We hence expect the average value of ϵ to be less than 2 when side-addition of chains occurs, and $\epsilon > 0$ since $\epsilon = 0$ is the condition for microgelation within a fixed volume.

From $\langle S^2 \rangle$ we can make the usual nondraining assumption that $\langle S^2 \rangle^{3/2}/M$ is proportional to $[\eta]$, so that the latter can be computed. Again, no attempt is made to adapt the model to the dimensions and masses of the PA reaction. Figure 9, nonetheless, shows $[\eta]$ vs M for $\epsilon = 1.5$, which captures the essential features of the slope of $[\eta]$ decreasing with M.

Except for the case of $\epsilon = 2$ (end-to-end addition of linear chains only), there is no single power law describing the dependence of $\langle S^2 \rangle$ on n, as seen in the figure. Also noteworthy is that $[\eta]$ can decrease with increasing M after a certain point, which is what we would expect for microgels.

Conclusions

The use of EDA in polyamine step-growth synthesis leads to a self-similar branched population for molar masses from around $10^4 - 10^6$ g/mol. This is seen in the constant relationship between M and $[\eta]$ over this range, furnished by GPC, and corresponds to the addition of monomeric EPI and linear chains to growing, branched structures. In the final divergent growth phase (FDGP), linear chains become scarce enough that ramifying growth reactions become significant. This results in an increase in the number of addition sites per polymer, causing mass-weighted, rather than number-weighted propagation. This leads to dramatic increases in polymer mass with each propagation reaction step, bimodal-

ity in the mass distribution, and changes in the relationship between M and $[\eta]$. The final result includes a high-mass mode of particles resembling 'microgels' that are qualitatively different than their branched precursors, with significantly higher polymer segment density, and the onset of whose growth is the precursor step to macroscopic gelation.

Besides the GPC data, the evidence for declaring the $M = 10^4 - 10^6$ mode to be branched resides in (1) the exponents $0.35 - 0.48$ in the viscosity/mass scaling relationship, (2) the low value of $[\eta]$ compared to other linear, water soluble polymers, (3) the abnormally low persistence length obtained if PA is *assumed* to be linear, (4) the -0.55 power law dependence of A_2 on M_w seen in the ACM experiments, and (5) the trend in log-$(r_{H,z})$ vs log M_w seen in the DLS data. The ACM experiments revealed the very strong polyelectrolyte behavior of PA and led to the ACOMP experiments being performed at moderately high ionic strength.

It was shown mathematically that mere asymmetrization (or bimodalization) of an initial monomodal population cannot produce the log $[\eta]_w$ vs log M_w observed if the M and $[\eta]$ relationship remains unchanged, i.e., the log $[\eta]_w$ vs log M_w behavior requires a change in polymer architecture, which occurs through the ramifying reactions.

Use of ACOMP as a monitoring technique hence reports not only the divergence of M_w leading to macroscopic gelation but also the ramifying growth reactions that lead to the leveling off, or even decrease in $[\eta]_w$. Although only a tentative ramifying model is proposed here, the application of ACOMP to branching reactions, in conjunction with more refined models, may allow for useful quantitative online monitoring of the nature of branching reactions. ACOMP may also prove useful in the long run for reaction control in the FDGP, signaling when a reaction should be quenched to optimize high M_w, while avoiding macroscopic gelation.

References and Notes

(1) Vorchheimer, N. Polyamines and Polyquaternary Ammonium Salts. In *Encyclopedia of Polymer Science and Engineering*, 2nd ed.; Mark, H., Bikales, N. M., Overberger, C. G., Menges, G., Eds.; John Wiley and Sons: NY 1988; Vol. 11, pp 489–507.
(2) Vorchheimer, N. Synthetic Polyelectrolytes. In *Polyelectrolytes for Water and Wastewater Treatment*; Schwoyer, W. L. K., Ed.; CRC Press: Boca Raton, FL, 1981; pp 1–45.
(3) Panzer, H. P.; Dixon, K. W. Polyquaternary flocculants. US Patent 28,807 (reissued), 1976.
(4) Florenzano, F. H.; Strelitzki, R.; Reed, W. F. *Macromolecules* **1998**, *31*, 7226.
(5) Grassl, B.; Alb, A. M.; Reed, W. F. *Macromol. Chem. Phys.* **2001**, *202*, 2518
(6) Grassl, B.; Reed, W. F. *Macromol. Chem. Phys.* **2002**, *203*, 586.
(7) Chauvin, F.; Alb, A. M.; Bertin, D.; Reed, W. F. *Macromol. Chem. Phys.* **2002**, *203*, 2029.
(8) Giz, A.; Giz, H.; Brousseau, J. L.; Alb, A. M.; Reed, W. F. *Macromolecules* **2001**, *34*, 1180.
(9) Giz, A.; Koc, A. O.; Giz, H.; Alb, A. M.; Reed, W. F. *Macromolecules* **2002**, *35*, 6557.
(10) Mignard, E.; Leblanc, T.; Bertin, D.; Guerret, O.; Reed, W. F. *Macromolecules* **2004**, *37*, 966.
(11) Reed, W. F. *Macromolecules* **2000**, *33*, 7165.
(12) Sorci, G. A.; Reed, W. F. *Langmuir* **2002**, *18*, 353.
(13) Bayly, E. E.; Brousseau, J.-L.; Reed, W. F. *Int. J. Polym. Anal. Charact.* **2002**, 7, 1.
(14) Sorci, G. A.; Reed, W. F. *Macromolecules* **2002**, *35*, 5218.
(15) Sorci, G. A.; Reed, W. F. *Macromolecules* **2004**, *37*, 554.
(16) Flory, P. J. *J. Am. Chem. Soc.* **1941**, *63*, 3096.
(17) Stockmayer, W. H. *J. Chem. Phys.* **1943**, *11*, 45.
(18) Zimm, B. H.; Stockmayer, W. H. *J. Chem. Phys.* **1949**, *17*, 1301.
(19) Burchard, W. *Adv. Polym. Sci.* **1999**, *143*, 113.
(20) Dobson, G. R., Gordon, M. *J. Chem. Phys.* **1964**, *43*, 705.
(21) Saito, O. In *The Radiation Chemistry of Macromolecules*; Dole, M., Ed.; Academic Press: New York, 1972.
(22) Peebles, L. H., Jr. *Molecular Weight Distributions in Polymers*; John Wiley and Sons: New York, 1971; Chapter 5.
(23) Tobita, H. *Macromol. Theory Simul.* **1996**, *5*, 547.
(24) Alexandorwicz, Z. *Phys. Rev. Lett.* **1985**, *54*, 1420.
(25) Yan, D.; Müller A. H. E.; Matyjaszewski, K. *Macromolecules* **1997**, *30*, 7024.
(26) Radke, W.; Litvinenko, G.; Müller, A. H. E. *Macromolecules* **1998**, *31*, 239.
(27) Hanselmann, R.; Hölter, D.; Frey, H. *Macromolecules* **1998**, *31*, 3790.
(28) Cheng, K. C. *Polymer* **2003**, *44*, 877.
(29) Flory, P. J. *J. Am. Chem. Soc.* **1941**, *63*, 3083.
(30) Dusek, K., M., Gordon, Ross-Murphy, S. B. *Macromolecules* **1978**, *11*, 236.
(31) Jones, R. A.; Cail, J. I.; Stepto, R, F. T.; Ward, I. M. *Macromolecules* **2000**, *33*, 7337.
(32) Cotts, P. M.; Guan, Z.; McCord, E.; McLain, S. *Macromolecules* **2000**, *33*, 6945.
(33) Podzimek, S.; Vlcek, T. *J. App. Polym. Sci.* **2001**, *82*, 454.
(34) Norwood, D. P.; Reed, W. F. *Int. J. Polym. Anal. Charact.* **1997**, *4*, 1.
(35) Berne, B.; Pecora, R. *Dynamic Light Scattering*; John Wiley and Sons: New York, 1978.
(36) Zimm, B. H. *J. Chem. Phys.* **1948**, *16*, 1093.
(37) Huggins, M. L. *J. Am. Chem. Soc.* **1942**, *64*, 2716.
(38) Burchard, W. *Adv. Polym. Sci.* **1999**, *143*, 113.
(39) Kulicke, W. M.; Kniewske, R.; Klein, J. *Prog. Polym. Sci.* **1982**, *8*, 379.
(40) Klein, J.; Conrad, K. D. *Makromol. Chem.* **1980**, *181*, 227.
(41) Tanford, C. *Physical Chemistry of Macromolecules*; Wiley: New York, 1961; Chapter 5.
(42) Reed, W. F In *Macroion Characterization*; Schmitz, K., Ed.; ACS Symposium Series 548; American Chemical Society: Washington, DC, 1994; pp 297–314.
(43) Yamakawa, H. *Modern Theory of Polymer Solutions*; Harper and Row: New York, 1971.
(44) Odijk, T. *J. Polym. Sci. Phys. Ed.* **1977**, *15*, 477.
(45) Skolnick, J.; Fixman, M. *Macromolecules* **1977**, *10*, 9444.
(46) Forster, S.; Schmidt, M. *Adv. Polym. Sci.* **1995**, *120*, 53.
(47) Dautzenberg, H.; Jaeger, W.; Kotz, J.; Philipp, B.; Seidel, Ch.; Stscherbina, D. *Polyelectrolytes: Formation, Characterization and Application*; Hanser Publishing: Munich, 1994.
(48) Although 'to ramify' and 'to branch' connote virtually no lexical difference in common English, 'ramifying growth' is chosen instead of 'cross-linking' to avoid the implication of macroscopic network formation.
(49) Zhu, S. *Macromolecules,* **1998**, *31*, 7519.
(50) Hidetaka, T. *Macromol. Theory Sim.* **1996**, *5*, 129.
(51) Pladis, P.; Kiparissides, C. *Chem. Eng. Sci.* **1998**, *53*, 3315.
(52) Iedema, P. D.; Wulkow, M.; Hoefsloot, H. C. J. *Macromolecules* **2000**, *33*, 7173.
(53) Lee, H. C.; Lee, W.; Chang, T.; Yoon, J. S.; Frater, D. J.; Mays, J. W. *Macromolecules* **1998**, *31*, 4114.
(54) Grcev, S.; Schoenmakers, P.; Iedema, P. *Polymer* **2004**, *45*, 39.
(55) Abrol, S.; Caulfield, M. J.; Qiao, G. G.; Solomon, D. H. *Polymer* **2001**, *42*, 5987.
(56) Koppel, D. E. *J. Chem. Phys.* **1972**, *11*, 4814.